2017

Effect of Various Carbonization Temperatures on ZIF-67 Derived Nanoporous Carbons

Yanna Guo
Waseda University, National Institute For Materials Science

Jing Tang
Hubei University, National Institute for Materials Science, Tsukuba, Waseda University

Rahul R. Salunkhe
National Institute for Materials Science, Japan, King Saud University

Zeid Abdullah Alothman
King Saud University

Md. Shahriar Al Hossain
University of Wollongong, National Institute For Materials Science, shahriar@uow.edu.au

See next page for additional authors

Publication Details

Guo, Y., Tang, J., Salunkhe, R. R., Alothman, Z. Abdullah., Hossain, M. A., Malgras, V. & Yamauchi, Y. (2017). Effect of Various Carbonization Temperatures on ZIF-67 Derived Nanoporous Carbons. Bulletin of the Chemical Society of Japan, 90 (8), 939-942.

Effect of Various Carbonization Temperatures on ZIF-67 Derived Nanoporous Carbons

Abstract
Here we have prepared ZIF-67 derived nanoporous carbons (NPCs) under different carbonization temperatures ranging from 800 to 1000 °C, and investigated the effect of the temperature on the porous structure. Raman analysis confirms that the graphitic degree of the obtained samples increases as the applied carbonization temperature is increased. With the gradual increase of the graphitic degree, the surface area is decreased.

Disciplines
Engineering | Physical Sciences and Mathematics

Publication Details
Guo, Y., Tang, J., Salunkhe, R. R., Alothman, Z. Abdullah., Hossain, M. A., Malgras, V. & Yamauchi, Y. (2017). Effect of Various Carbonization Temperatures on ZIF-67 Derived Nanoporous Carbons. Bulletin of the Chemical Society of Japan, 90 (8), 939-942.

Authors
Yanna Guo, Jing Tang, Rahul R. Salunkhe, Zeid Abdullah Alothman, Md. Shahriar Al Hossain, Victor Malgras, and Yusuke Yamauchi

Selected Paper

Effect of Various Carbonization Temperatures on ZIF-67 Derived Nanoporous Carbons

Yanna Guo,[1,2,†] Jing Tang,[1,†] Rahul R. Salunkhe,[1] Zeid Abdullah Alothman,[3] Md. Shahriar A. Hossain,[1,4] Victor Malgras,*[1] and Yusuke Yamauchi*[1,2,4]

[1]International Center for Materials Nanoarchitectonics (MANA), National Institute for Materials Science (NIMS), 1-1 Namiki, Tsukuba, Ibaraki 305-0044

[2]Faculty of Science and Engineering, Waseda University, 3-4-1 Okubo, Shinjuku, Tokyo 169-8555

[3]Advanced Materials Research Chair, Chemistry Department, College of Science, King Saud University, Riyadh 11451, Saudi Arabia

[4]Australian Institute for Innovative Materials (AIIM), University of Wollongong, North Wollongong, NSW 2500, Australia

E-mail: yamauchi.yusuke@nims.go.jp, yusuke@uow.edu.au

Received: April 15, 2017; Accepted: May 11, 2017; Web Released: July 12, 2017

Yusuke Yamauchi

After receiving his Ph.D. in 2007 from Waseda University (Japan), Yusuke Yamauchi joined NIMS to establish his own research group. In 2016, he joined the University of Wollongong as a full professor. He concurrently serves as group leader in NIMS, visiting/guest professor at several universities (Waseda University, Tianjin University, King Saud University), and associate editor of APL Materials published by the American Institute of Physics (AIP). Prof. Yamauchi has published more than 500 papers in international refereed journals with around 20,000 citations (*h*-index > 70) and was selected as one of the Highly Cited Researchers in Chemistry (Thomson Reuters) in 2016.

Abstract

Here we have prepared ZIF-67 derived nanoporous carbons (NPCs) under different carbonization temperatures ranging from 800 to 1000 °C, and investigated the effect of the temperature on the porous structure. Raman analysis confirms that the graphitic degree of the obtained samples increases as the applied carbonization temperature is increased. With the gradual increase of the graphitic degree, the surface area is decreased.

1. Introduction

Nanoporous materials are promising candidates for several applications ranging from catalytic supports toward water treatment to electrode materials for batteries, fuel cells, and supercapacitors, and drug delivery carriers.[1] Among many compositions, nanoporous carbon (NPC) materials have recently attracted great interests due to their unique physical and chemical properties, like excellent chemical and mechanical stability, good electrical conductivity, and high specific surface area.[2] While mesoporous carbons with ordered porous arrangements have been extensively studied to date, metal-organic framework (MOF)-derived NPCs with unique pore structures have been recently becoming a research hotspot.[3]

The mostly adopted strategy for the synthesis of porous carbons is the hard-templating method, in which a broad variety of porous materials can be selected to act as molds.[4] This templating process has the advantage of precisely controlling the morphology and average pore size. However, the complicated steps involved in the preparation of the starting template materials (carbonization inside the pores and removal of the template matrix) are limiting its implementation in large-scale industrial production. In recent years, MOFs or porous coordination polymers (PCPs), which are formed by assembling metal ions with organic ligands, have attracted a great interest.[5] Motivated by their fascinating properties, such as high surface area, as well as tunable chemical compositions and textures, several types of MOFs have been utilized as precursors for the preparation of NPCs,[6,7] acting both as sacrificial template and secondary carbon precursor. Compared with the above-mentioned hard-templating method, this approach is relatively simple.

Previously, NPCs have been successfully synthesized from zeolitic imidazolate framework precursors (e.g., ZIF-8).[8] Zeolitic imidazolate frameworks (ZIFs) comprise a well-known

† These authors equally contributed to this work.

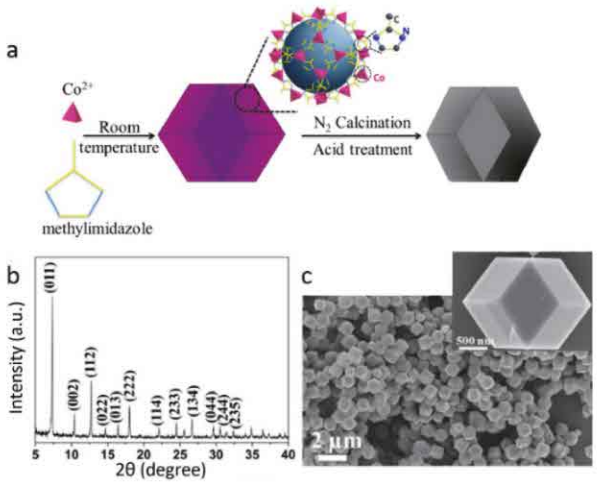

Figure 1. (a) Schematic illustration of the synthesis of nanoporous carbons. (b) Wide-angle XRD pattern and (c) SEM image of the ZIF-67 crystals. Inset in (c) shows a high-magnification SEM image of an isolated ZIF-67 crystal.

subfamily of MOFs formed through the coordination between metal ions and imidazole derivatives. Compared to ZIF-8, ZIF-67 contains Co species which are converted into metalic Co during the carbonization process. These deposited Co nanoparticles can act as catalysts for the graphitization of carbon.[9] Therefore, by adjusting the applied carbonization temperature, we can control the degree of graphitization of the materials, which finally determines the material properties. In this work, we carefully study the effect of the applied carbonization temperature on the surface area, pore size distribution, and graphitization degree of NPCs (Figure 1a).

2. Experimental

Chemicals. Cobalt nitrate hexahydrate ($Co(NO_3)_2 \cdot 6H_2O$, 99%) was purchased from Sigma-Aldrich Chemical Co. 2-Methylimidazole (MeIm, purity 99%), hydrofluoric acid, and methanol were obtained from Nacalai Tesque Reagent Co. All chemicals were used without further purification.

Synthesis of ZIF-67 Derived Carbons. The preparation of ZIF-67 crystals was adapted from our previously reported synthetic method.[10] Cobalt nitrate hexahydrate (0.87 g) was dissolved in methanol (30 mL), while 2-methylimidazole (0.98 g) was dissolved in methanol (10 mL). The two solutions were then mixed together and stirred vigorously for 5 min. The mixture was aged at room temperature for 12 h, after which the precipitate (ZIF-67) was collected, separated by centrifugation, washed carefully with methanol, and dried at 80 °C. The NPCs were obtained after carbonizing the ZIF-67 crystals under nitrogen flow at temperatures ranging from 800 to 1000 °C for 2 h with a heating rate of $2\,°C \cdot min^{-1}$. The resulting NPCs containing small Co nanoparticles were washed extensively with a HF solution (10 wt %) in order to remove any trace of metals. The obtained carbons are denoted as C-*n*, where *n* represents the carbonization temperature.

Characterization. Scanning electron microscopy (SEM) images were obtained with a Hitachi SU-4800 microscope at an accelerating voltage of 5 kV. Transmission electron microscope (TEM) and high-angle annular dark-field scanning transmission electron microscope (HAADF-STEM) observations were performed using a JEM-2010F system operating at 200 kV. Wide-angle powder X-ray diffraction (XRD) patterns were measured using a Rigaku RINT 2000 X-ray diffractometer using monochromated CuKα radiation (40 kV, 40 mA) at a scanning rate of $2\,°C \cdot min^{-1}$. Raman spectra were measured using a Horiba-Jobin-Yvon T64000 (Photon Design). Nitrogen adsorption–desorption analysis was performed using a Quanta Chrome Autosorb Automated Gas Sorption System at 77 K. The total pore-size distributions were calculated from the adsorption branches of the isotherms based on the non-localized density functional theory (NLDFT) method.

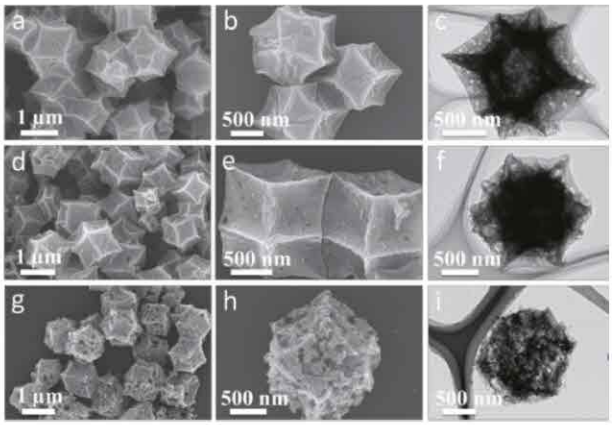

Figure 2. SEM and TEM images of the NPCs prepared at different temperatures [(a–c) 800 °C, (d–f) 900 °C, and (g–i) 1000 °C].

3. Results and Discussion

The obtained ZIF-67 crystals were characterized by XRD and SEM. The XRD pattern (Figure 1b) shows that all the peaks can be indexed to the standard simulated pattern of ZIF-67 without any impurities.[10] The SEM images (Figure 1c and inset) reveal that the well-dispersed ZIF-67 crystals have a typical rhombic dodecahedral morphology, and an average particle size ranging from 1 to 2 μm.

During the carbonization process of the ZIF-67, the Co species tend to aggregate, thus forming metallic nanoparticles (Figure S1). Wide-angle XRD patterns for ZIF-67 derived carbon samples before the HF treatment are shown in Figure S2. With increasing the applied temperature, the intensity and sharpness of the peaks corresponding to face-centered-cubic (*fcc*) Co crystals gradually increases. Using the Scherrer equation, the average crystallite size was estimated to be around 27 nm (for 800 °C), 38 nm (for 900 °C), and 42 nm (for 1000 °C).

Figure 2 shows the SEM and TEM images for all the NPCs after ZIF-67 carbonization followed by HF treatment. The overall particle size and shape of the original ZIF-67 precursor were retained, although the surface appeared distorted and bumpy after carbonization. Highly magnified SEM images of the samples show higher degrees of distortion and the appearance of surface porosity, especially at higher carbonization temperature.

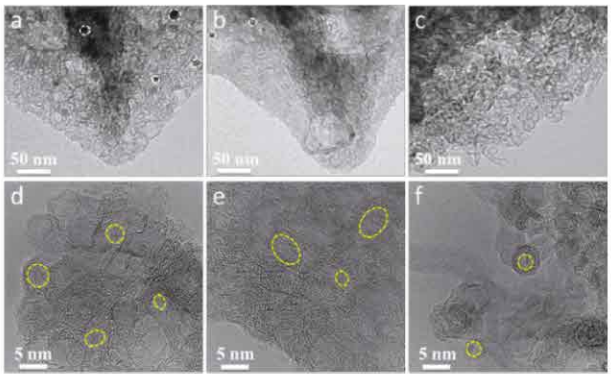

Figure 3. Low- and high-magnification TEM images of the NPCs, after HF treatment, prepared at different temperatures [(a, d) 800 °C, (b, e) 900 °C, and (c, f) 1000 °C]. The deposited Co nanoparticles are indicated by white circles in the low-magnification TEM images, while the formed mesopores in the chemically etched samples are indicated by yellow circles in high resolution TEM images.

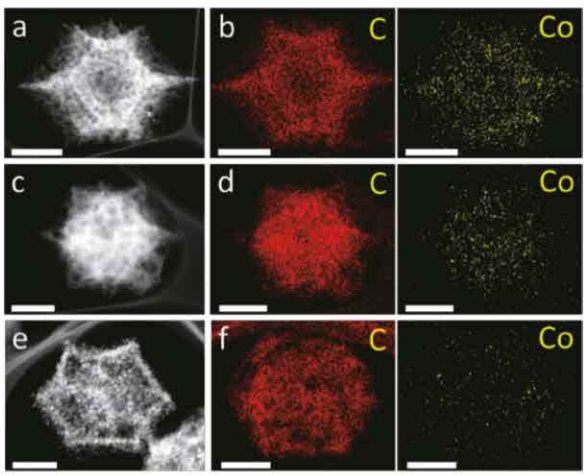

Figure 4. HAADF-STEM images and elemental mappings of NPCs prepared at different temperatures [(a, b) 800 °C, (c, d) 900 °C, and (e, f) 1000 °C]. The scale bars are 500 nm.

High-resolution TEM (HRTEM) images (Figure 3) provide more details about the structure of the samples prepared at different temperatures. It was found that all the samples showed porous structures with a high degree of graphitization. During the carbonization process, the Co nanoparticles can act as a catalyst to assist the graphitization of carbon.[9,10] Figure 3a-c revealed that most of the Co nanoparticles were removed by chemical etching. At relatively low sintering temperature, however, some Co nanoparticles are still present. With increasing the temperature, most of the Co nanoparticles are efficiently removed from the carbon matrix. The results from the elemental mapping analysis (Figure 4) are consistent with the TEM observations. The content of elemental Co gradually decreases as the calcination temperature increases. The Co content for each sample was 2.5% (for C-800), 0.3% (for C-900), and <0.1% (C-1000). All the samples are treated with the same acidic solution, the only difference being the applied carbonization temperature. As shown in Figure 2g-i, the surface

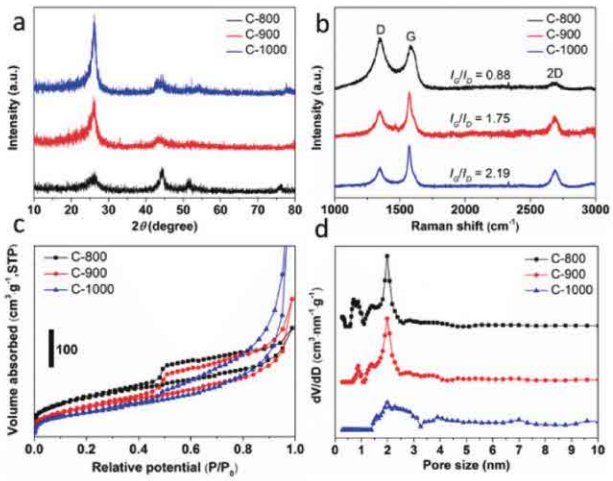

Figure 5. (a) Wide-angle XRD patterns, (b) Raman spectra, (c) N_2 adsorption–desorption isotherms, and (d) NLDFT pore-size distributions of NPCs prepared at different temperatures (800 °C, 900 °C, and 1000 °C).

structure tends to collapse at higher temperature, and the Co nanoparticles are etched more efficiently.

The crystalline structure of the NPCs was analyzed by XRD. As revealed in Figure 5a, all the samples undergo structural transformation after carbonization. By increasing the temperature up to 1000 °C, the diffraction peak at around 25°, which is representative of the characteristic carbon (002) interlayer, becomes sharper and more intense, implying the formation of carbon with a higher degree of graphitization. On the other hand, the (111) and (200) diffractions of the *fcc* Co crystal located at 44.2° and 51.6°, respectively, can still be observed, because some Co nanoparticles are still present even after HF treatment.[9] The peaks become weaker as the temperature is increased, which is in accordance with the elemental mapping analysis (Figure 4).

Raman spectroscopy was also conducted to investigate the structural characterization of samples obtained at different carbonization temperatures. As seen in Figure 5b, two peaks located at around 1350 and 1580 cm^{-1}, which can be indexed to the disorder-induced (D) and graphite (G) peaks of carbon materials, respectively, are observed. The relative intensity ratios of G to D bands (I_G/I_D) become larger as the temperature increases, implying that the graphitization degree of carbon increases. Moreover, the intensity of the 2D band arising from the overtone of the D band at around 2700 cm^{-1} becomes stronger at higher temperatures, which further confirms that graphitic structures are well-developed. Interestingly, the HRTEM data for C-1000 (Figure 3c, 3f and S3) shows that carbon nanotubes (CNTs), of a few hundred nanometers in length, grew on the particle surface. The graphitic carbon structure is known to have higher electrical conductivity than amorphous carbon. Such a CNT-rich surface can form electrically conductive bridges between the NPC particles and play an important role for several electrical applications.[11]

To investigate the variation of specific surface areas and pore size distributions between the samples carbonized at different temperatures, N_2 adsorption–desorption analysis has been carried out at 77 K (Figure 5c). All the samples exhibit steep

increases at very low relative pressure, indicating the presence of micropores. For $P/P_0 > 0.2$, the isotherms exhibit a slight capillary condensation, corresponding to the presence of mesopores with different sizes. The specific surface areas of the samples are 337 $m^2 \cdot g^{-1}$ (for 800 °C), 260 $m^2 \cdot g^{-1}$ (for 900 °C) and 205 $m^2 \cdot g^{-1}$ (for 1000 °C). These surface areas are not as high as our previously reported NPCs derived from ZIF-67 prepared by a different method.[9] The pore-size distribution determined by NLDFT calculation is plotted in Figure 5d. The obtained samples exhibit both micropores and mesopores. The pore-size distribution becomes broader and slightly shifted towards larger pore diameters as the carbonization temperature increases. The ~0.8 nm micropores, comparable to the ZIF-68 parent precursor, mostly vanish after carbonization at 1000 °C.

4. Conclusion

Nanoporous carbons were successfully obtained through a one-step process. After carbonization at different temperatures, the samples showed different chemical and physical properties. It highlights how the pore-size distribution, surface area and graphitic degree can simply be tuned by changing the carbonization temperature. This work provides new insights regarding the design optimization of nanoporous carbon materials using MOFs as precursor.

This work was partly supported by an Australian Research Council (ARC) Future Fellow (FT150100479), the AIIM-MANA 2016 grant, and JSPS KAKENHI Grant Number 17H05393 (Coordination Asymmetry). Y.Y and Z.A.A. are grateful to the Deanship of Scientific Research, King Saud University for funding through Vice Deanship of Scientific Research Chairs.

Supporting Information

Contains additional TEM and XRD data. This material is available on http://dx.doi.org/10.1246/bcsj.20170138.

Reference

1 a) T. Yamada, M. Sadakiyo, A. Shigematsu, H. Kitagawa, *Bull. Chem. Soc. Jpn.* **2016**, *89*, 1. b) V. Malgras, Q. Ji, Y. Kamachi, T. Mori, F.-K. Shieh, K. C.-W. Wu, K. Ariga, Y. Yamauchi, *Bull. Chem. Soc. Jpn.* **2015**, *88*, 1171. c) Z. Huang, S. Che, *Bull. Chem. Soc. Jpn.* **2015**, *88*, 617.

2 a) K. Sakaushi, M. Antonietti, *Bull. Chem. Soc. Jpn.* **2015**, *88*, 386. b) M. P. Adhikari, R. Adhikari, R. G. Shrestha, R. Rajendran, L. Adhikari, P. Bairi, R. R. Pradhananga, L. K. Shrestha, K. Ariga, *Bull. Chem. Soc. Jpn.* **2015**, *88*, 1108. c) H. Tabuchi, K. Urita, I. Moriguchi, *Bull. Chem. Soc. Jpn.* **2015**, *88*, 1378. d) J. Tang, J. Liu, N. L. Torad, T. Kimura, Y. Yamauchi, *Nano Today* **2014**, *9*, 305. e) H. Kumagai, K. Takanabe, J. Kubota, K. Domen, *Bull. Chem. Soc. Jpn.* **2015**, *88*, 584. f) Y. Li, H. Tan, R. R. Salunkhe, J. Tang, L. K. Shrestha, B. P. Bastakoti, H. Rong, T. Takei, J. Henzie, Y. Yamauchi, K. Ariga, *Chem. Commun.* **2017**, *53*, 236. g) W. Zhang, X. Jiang, Y. Zhao, A. Carné-Sánchez, V. Malgras, J. Kim, J. H. Kim, S. Wang, J. Liu, J.-S. Jiang, Y. Yamauchi, M. Hu, *Chem. Sci.* **2017**, *8*, 3538. h) W. Zhang, X. Jiang, X. Wang, Y. V. Kaneti, Y. Chen, J. Liu, J.-S. Jiang, Y. Yamauchi, M. Hu, *Angew. Chem., Int. Ed.* **2017**, doi:10.1002/anie.201701252.

3 a) J. Tang, Y. Yamauchi, *Nat. Chem.* **2016**, *8*, 638. b) R. R. Salunkhe, Y. V. Kaneti, J. Kim, J. H. Kim, Y. Yamauchi, *Acc. Chem. Res.* **2016**, *49*, 2796.

4 a) J. Lee, S. Han, T. Hyeon, *J. Mater. Chem.* **2004**, *14*, 478. b) S. Jun, S. H. Joo, R. Ryoo, M. Kruk, M. Jaroniec, Z. Liu, T. Ohsuna, O. Terasaki, *J. Am. Chem. Soc.* **2000**, *122*, 10712.

5 a) J. R. Long, O. M. Yaghi, *Chem. Soc. Rev.* **2009**, *38*, 1213. b) Y. Tanihara, A. Nozaki, Y. Kuwahara, K. Mori, H. Yamashita, *Bull. Chem. Soc. Jpn.* **2016**, *89*, 1048. c) M. Ishidoshiro, H. Imoto, K. Naka, *Bull. Chem. Soc. Jpn.* **2016**, *89*, 1057.

6 a) B. Liu, H. Shioyama, T. Akita, Q. Xu, *J. Am. Chem. Soc.* **2008**, *130*, 5390. b) H.-L. Jiang, B. Liu, Y.-Q. Lan, K. Kuratani, T. Akita, H. Shioyama, F. Zong, Q. Xu, *J. Am. Chem. Soc.* **2011**, *133*, 11854.

7 a) W. Chaikittisilp, K. Ariga, Y. Yamauchi, *J. Mater. Chem. A* **2013**, *1*, 14. b) M. Hu, J. Reboul, S. Furukawa, N. L. Torad, Q. Ji, P. Srinivasu, K. Ariga, S. Kitagawa, Y. Yamauchi, *J. Am. Chem. Soc.* **2012**, *134*, 2864.

8 a) N. L. Torad, M. Hu, Y. Kamachi, K. Takai, M. Imura, M. Naito, Y. Yamauchi, *Chem. Commun.* **2013**, *49*, 2521. b) C. Young, R. R. Salunkhe, J. Tang, C.-C. Hu, M. Shahabuddin, E. Yanmaz, M. S. A. Hossain, J. H. Kim, Y. Yamauchi, *Phys. Chem. Chem. Phys.* **2016**, *18*, 29308. c) N. L. Liu, S. Dutta, R. R. Salunkhe, T. Ahamad, S. M. Alshehri, Y. Yamauchi, C.-H. Hou, K. C.-W. Wu, *Sci. Rep.* **2016**, *6*, 28847. d) R. R. Salunkhe, C. Young, J. Tang, T. Takei, Y. Ide, N. Kobayashi, Y. Yamauchi, *Chem. Commun.* **2016**, *52*, 4764.

9 a) N. L. Torad, M. Hu, S. Ishihara, H. Sukegawa, A. A. Belik, M. Imura, K. Ariga, Y. Sakka, Y. Yamauchi, *Small* **2014**, *10*, 2096. b) J. Tang, R. R. Salunkhe, J. Liu, N. L. Torad, M. Imura, S. Furukawa, Y. Yamauchi, *J. Am. Chem. Soc.* **2015**, *137*, 1572.

10 N. L. Torad, R. R. Salunkhe, Y. Li, H. Hamoudi, M. Imura, Y. Sakka, C. C. Hu, Y. Yamauchi, *Chem.—Eur. J.* **2014**, *20*, 7895.

11 J. Kim, C. Young, J. Lee, M. S. Park, M. Shahabuddin, Y. Yamauchi, J. H. Kim, *Chem. Commun.* **2016**, *52*, 13016.